Article

3D-printed machines that manipulate microscopic objects using capillary forces

https://doi.org/10.1038/s41586-022-05234-7

Received: 24 October 2021

Accepted: 11 August 2022

Published online: 26 October 2022

Check for updates

Cheng Zeng[1,8], Maya Winters Faaborg[1,8], Ahmed Sherif[1], Martin J. Falk[2], Rozhin Hajian[1,3], Ming Xiao[1,4], Kara Hartig[5], Yohai Bar-Sinai[1,6,7], Michael P. Brenner[1,5] & Vinothan N. Manoharan[1,5]✉

Objects that deform a liquid interface are subject to capillary forces, which can be harnessed to assemble the objects[1–4]. Once assembled, such structures are generally static. Here we dynamically modulate these forces to move objects in programmable two-dimensional patterns. We 3D-print devices containing channels that trap floating objects using repulsive capillary forces[5,6], then move these devices vertically in a water bath. Because the channel cross-sections vary with height, the trapped objects can be steered in two dimensions. The device and interface therefore constitute a simple machine that converts vertical to lateral motion. We design machines that translate, rotate and separate multiple floating objects and that do work on submerged objects through cyclic vertical motion. We combine these elementary machines to make centimetre-scale compound machines that braid micrometre-scale filaments into prescribed topologies, including non-repeating braids. Capillary machines are distinct from mechanical, optical or fluidic micromanipulators in that a meniscus links the object to the machine. Therefore, the channel shapes need only be controlled on the scale of the capillary length (a few millimetres), even when the objects are microscopic. Consequently, such machines can be built quickly and inexpensively. This approach could be used to manipulate micrometre-scale particles or to braid microwires for high-frequency electronics.

Our aim is to use capillary forces to programme the motion of floating objects instead of their static configurations. To this end, we vary the shape of the boundary around the floating objects instead of manipulating the shapes of the objects themselves. The boundary is a plastic device that we 3D-print. Its wettability can be controlled to create repulsive capillary forces between the plastic and the floating objects.

To demonstrate the concept, we print a hollow, centimetre-scale channel, fill it with water, and place a millimetre-scale silicone disk (a 'float') at the air–water interface. Although the float is denser than water, it pins the contact line at its top edge and remains suspended by the interfacial tension. Near the float, the interface bends downwards (Fig. 1a,b). Near the wall, which we make hydrophilic (Supplementary Methods), the interface bends upwards. Displacing the float from the centre of the channel results in a restoring force, which arises from the increase in interfacial and gravitational potential energy (Fig. 1c and Supplementary Discussion). Thus, much like an optical tweezer[7,8], the channel acts as a 'capillary tweezer' that traps an object without solid contact.

The tweezer can also steer the object in the plane of the interface. We steer the float by moving the channel vertically rather than laterally. If the cross-section of the channel changes with height, the float 'sees' a boundary that changes with time. Repulsion from this changing boundary moves the float.

Elementary capillary machines

To translate the float, we print a sloping channel and move it vertically with respect to the interface. The float responds by moving linearly in the plane of the interface (Fig. 1d,e and Supplementary Video 1). We move the machine slowly (about 1 mm s^{-1}) so that the dynamics are effectively quasistatic, and inertial and hydrodynamic effects are not relevant.

We have thus described a simple machine that, like a screw or lever, modifies the direction and magnitude of forces. This capillary machine converts vertical motion to horizontal motion of the float, with the fluid interface serving as the linkage.

Compared to moving the tweezer laterally to steer the float, encoding the path of the float into the shape of the channel is mechanically simpler: only one motorized degree of freedom (z, the height of the machine relative to the interface) is needed to steer the float in two dimensions. Additional complexity can be built into the machine at no additional mechanical cost. For example, two floats can be trapped in two separate channels, and both floats can be translated independently using the same, single motorized degree of freedom.

To coordinate the motion of multiple floats, we take advantage of the capillary attraction[9] between them. The machine in Fig. 2a converts vertical motion to rotation of two floats. The two floats attract each other,

[1]Harvard John A. Paulson School of Engineering and Applied Sciences, Harvard University, Cambridge, MA, USA. [2]Department of Physics, University of Chicago, Chicago, IL, USA. [3]Department of Mechanical Engineering, University of Massachusetts Lowell, Lowell, MA, USA. [4]College of Polymer Science and Engineering, Sichuan University, Chengdu, China. [5]Department of Physics, Harvard University, Cambridge, MA, USA. [6]School of Physics and Astronomy, Tel Aviv University, Tel Aviv, Israel. [7]Center for Physics and Chemistry of Living Systems, Tel Aviv University, Tel Aviv, Israel. [8]These authors contributed equally: Cheng Zeng, Maya Winters Faaborg. ✉e-mail: vnm@seas.harvard.edu

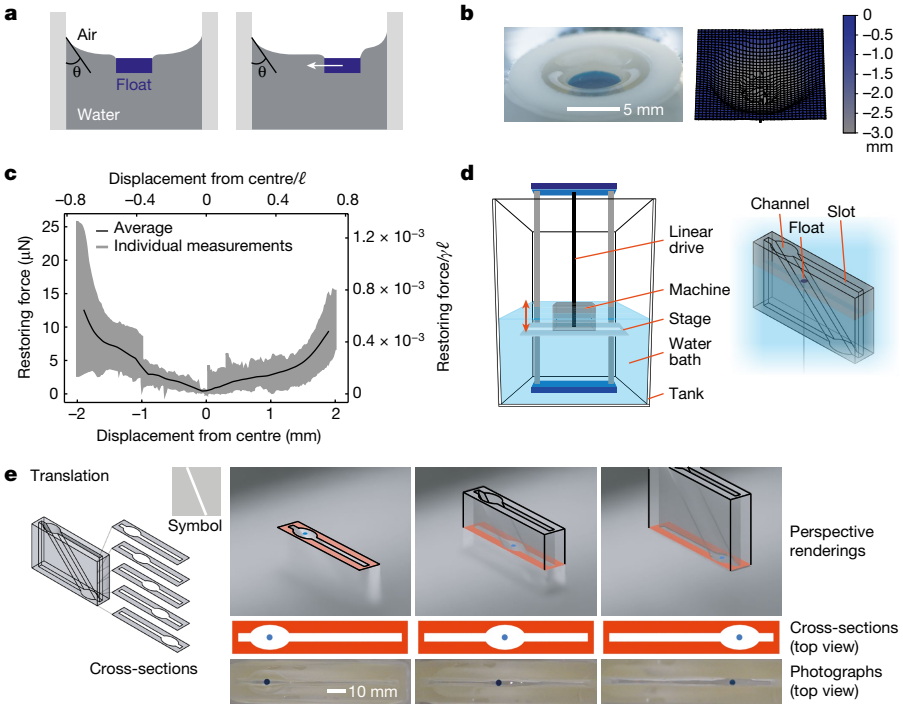

Fig. 1 | Trapping and steering objects using repulsive capillary forces. **a**, Diagram of meniscus formed when water fills a hydrophilic channel with contact angle θ. The float—a piece of polydimethylsiloxane (PDMS), which is denser than water—pins the interface and bends it downwards. When the float is displaced from the centre of the channel, the height of the float and the interfacial energy increase, leading to a restoring force (white arrow). **b**, Photograph of the meniscus and float (blue; weight 25 mg) in a 3D-printed channel (left) and plot of height of the interface in a similar channel, as measured by laser profilometry, showing curvature of meniscus (right; float diameter 4 mm, weight 30.6 mg). **c**, Measured restoring force (right axis, relative to the product of surface tension γ and capillary length ℓ) as a function of displacement of the fibre (top axis, relative to ℓ) along the long dimension of an elliptical channel with 9-mm semi-major axis and 6-mm semi-minor axis. The grey area shows the range of individual measurements, and the solid black line is a moving average with a 0.4-mm window size. **d**, Diagram of motorized stage and bath used to move a machine (inset). **e**, A machine with a sloping channel (cross-sections shown at left) can be used to translate a float along the interface. As the translator moves vertically relative to the water (perspective renderings at top), repulsive capillary forces push the float (blue circle) away from the walls, translating it horizontally (top-view renderings at centre). Photographs (bottom) of the machine taken from above show the float moving as the height of the machine changes. The slot seen in the cross-sections enables a submerged object to be attached to the float.

and the pair then aligns with the long axis of the channel to minimize repulsion from the walls (Supplementary Video 2). To separate two round floats after rotation, we use a machine with wedges along the walls (Fig. 2b), which introduce a repulsive capillary force that pushes the floats apart without physical contact (Supplementary Video 3).

These three elementary machines—the translator, rotator and separator—can be combined to perform more complex operations. The resulting compound machines can apply forces and torques to multiple floats, enabling them to be steered in prescribed two-dimensional patterns programmed into the geometry of the channels. But each of these operations is reversible: if the vertical motion of a compound machine is reversed, the floats follow the same paths in reverse.

We therefore add a fourth elementary machine that breaks path-reversal symmetry, enabling us to convert cyclic motion to work, as in an engine. If the lateral symmetry of two joined channels is broken (Fig. 2c), a float fed through the smaller channel enters the larger channel when the direction is reversed (Fig. 2c and Supplementary Video 4). When a capillary machine with such asymmetric junctions at its top and bottom is operated cyclically—reversing direction whenever the interface is at the height of the junctions—the floats follow different paths on the up and down strokes. Two patterns of motion can therefore be programmed into the same machine. The pattern is selected by the direction of motion.

Braiding machines

A natural application of these machines is making braids, because when all rotations are ±180°, the paths traced by the floats in time are in the mathematical n-braid group[10]. This group consists of all ways in which the positions of n unidirectional paths or strands can be interchanged. Any braid can be decomposed into swaps σ_i and σ_i^{-1}, corresponding to moving the strand in position i over (σ_i) or under (σ_i^{-1}) the strand in position $i+1$. The braid is defined by a series of swaps called the 'braid word'. In our capillary machines, the paths of two floats can be swapped using translators, rotators and separators. Braid words with repeating units can be encoded by incorporating asymmetric junctions and operating the machine cyclically.

We combine the four elementary machines to make a braiding machine (Fig. 3a) that creates a twist-free, three-strand braid out of microscale fibres. To convert the paths of the floats into a physical braid, we attach the top of each fibre to a needle piercing each float (Fig. 3b). To enable the needles to move unencumbered, we add a slot that extends through the machine (for the same reason, we include a slot in the elementary machines in Figs. 1 and 2). As the machine moves up, the floats trace the path $\sigma_1\sigma_2^{-1}$, as do the tops of the fibres (Fig. 3c,d). As the machine moves down, the floats do not swap (Fig. 3d). Their paths correspond to the identity operator $\mathbf{I}$. Thus, in one complete cycle, the machine creates one unit $(\sigma_1\sigma_2^{-1}\mathbf{I})$ of a repeating braid. Numerical calculations of the positions of the floats agree well with measurements (Fig. 3e and Supplementary Methods).

By cycling the machine m times we make a braid with braid word $(\sigma_1\sigma_2^{-1}\mathbf{I})^m = (\sigma_1\sigma_2^{-1})^m$, where m is the number of repeating units (Fig. 3f and Supplementary Video 5). In principle, the machine can make a braid with any m. In practice, m is limited by the tension that the

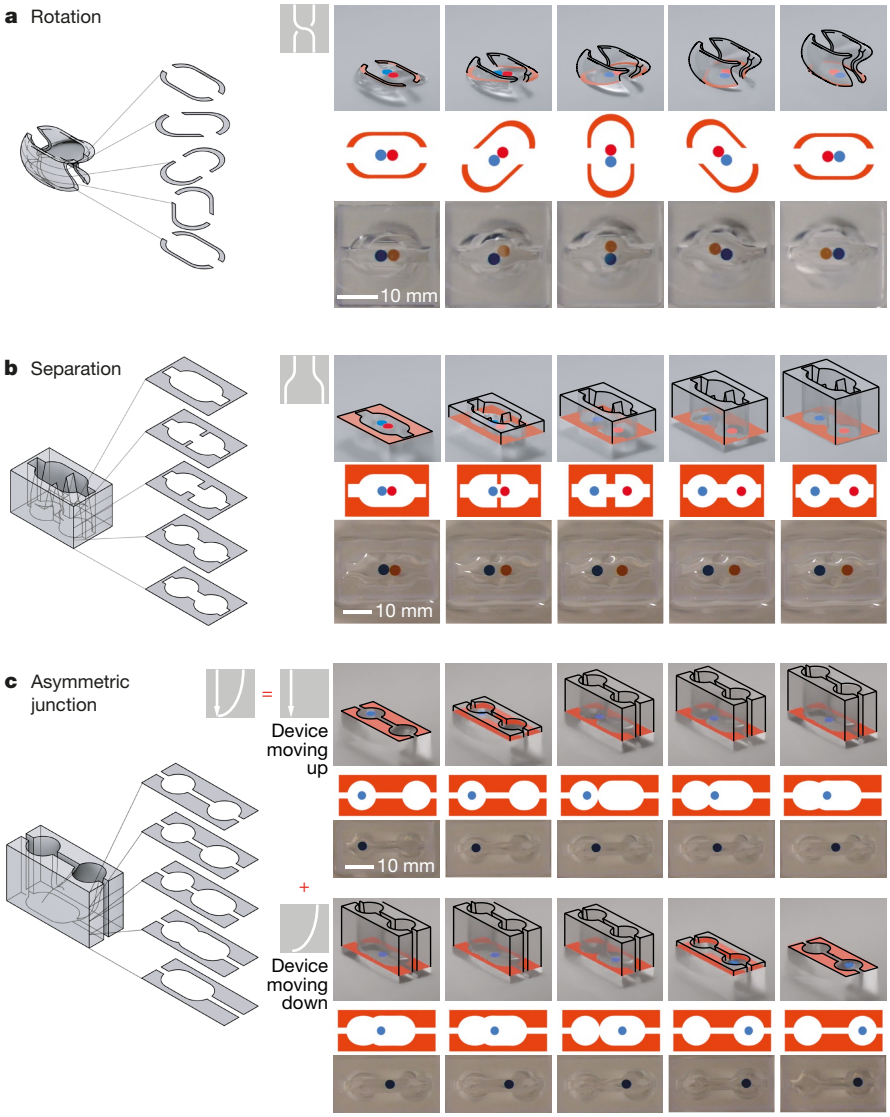

Fig. 2 | Elementary capillary machines enable multiple floats to be steered in complex patterns. Each panel shows cross-sections of the machine (left), perspective renderings of the machine moving relative to the interface (top right), top-view renderings of the machine cross-sections at the interface (middle right), and photographs taken from above a moving machine (bottom right). **a**, A machine to rotate two floats about a central axis consists of a channel with oval cross-sections. As the machine moves up, repulsive capillary forces from the walls apply a torque to a pair of floats (blue and red circles) joined by attractive capillary forces. **b**, A machine to separate two joined floats consists of a channel with wedged protrusions on two sides. As the machine moves up, capillary repulsion from the wedges pushes the floats apart. **c**, A machine that enables a float to take two different paths, depending on the direction of motion, joins two channels with different widths. As the machine moves up, a float in the smaller channel exits into the centre of the junction. Reversing the motion of the machine causes the float to enter the larger channel, where it can remain further from the walls.

growing braid exerts on the floats, which eventually inhibits their motion or submerges them.

We use this machine to braid fibres with diameters less than 10 μm (Fig. 3g). Industrial maypole braiding machines[11,12] cannot easily make such 'microbraids', as evidenced by the many new microbraiding technologies that have been proposed[13–18]. Such technologies either require a micromanipulator[13,17] or have a complex mechanical design[14–16,18]. Other techniques based on self- or directed assembly produce helical, twisted or plied fibres[19–21]. In comparison, a capillary braiding machine has a simple mechanical design and can produce braids not limited to twists or plies.

Braiding using hysteresis and switching

Although in principle one can 3D-print a machine corresponding to any desired braid word, there are two difficulties with such an approach. First, the machine becomes bulky as the number of fibres or wires increases, because each swap requires a rotator and asymmetric junctions. Second, a different machine is needed for each braid topology.

To address the first difficulty—keeping the machine compact—we develop a ratchet that rotates the floats and breaks path-reversal symmetry, thereby replacing a rotator and two asymmetric junctions. To do this, we take advantage of the difference in contact angle when water advances or recedes on the 3D-printed plastic (Fig. 4a). The effects of this contact-angle hysteresis[22] depend sensitively on the advancing and receding contact angles and on geometry, but the behaviour can be modelled and predicted (Supplementary Methods). We use simulations to design a ratchet (Fig. 4b) that rotates a rectangular float on the down stroke but not on the up stroke (Supplementary Video 6). The symmetry breaks because the contact angle controls whether the float tends to align with the slot or with the rectangular channel.

We use the ratchet to make a compact (2-cm tall) machine that twists micrometre-scale fibres as it cycles (Fig. 4c) and a three-strand braiding

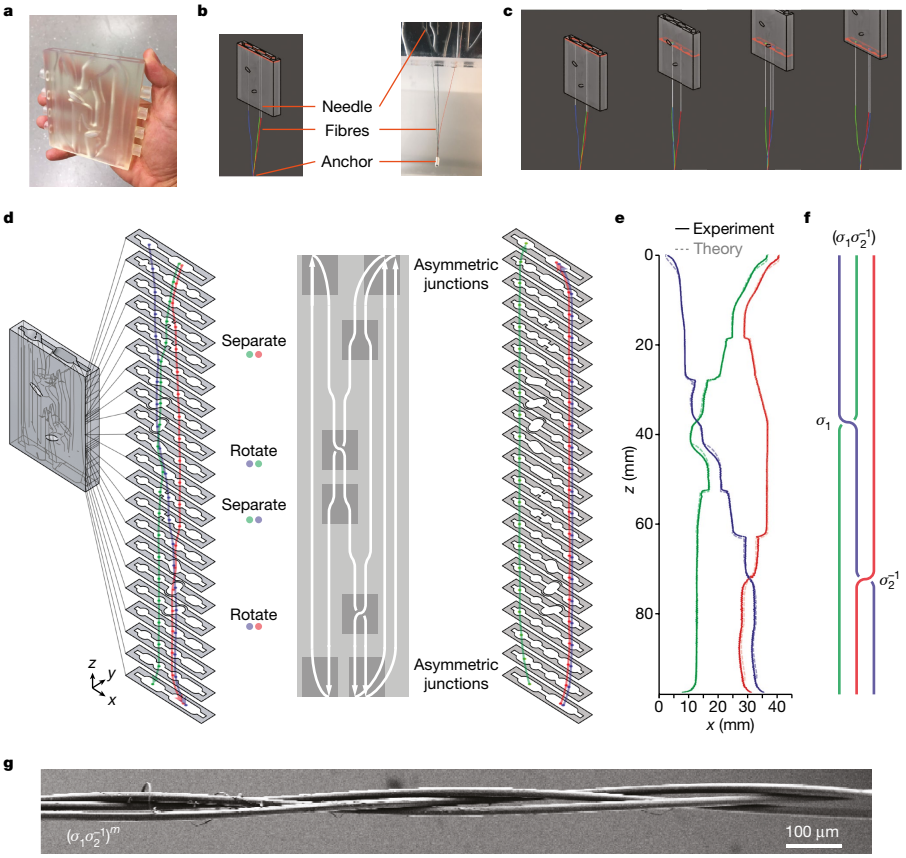

Fig. 3 | A capillary machine that can braid three microscopic fibres. **a**, Photograph of machine for making a three-stranded braid with no twist, like a typical hair braid. **b**, Diagram showing submerged fibres attached to the floats by stainless steel needles, which extend through the slots of the machine. The slots allow the needles to move freely, transferring the motion of the floats to the attached fibres. **c**, Animation of braid formation as machine moves up and down in water (see Supplementary Video 5). **d**, Diagram of machine showing cross-sections and the paths traced by the floats during each stroke (up or down). The machine consists of translators, rotators, separators and asymmetric junctions (central schematic). The asymmetric junctions enable the floats to trace different paths and tighten the braid after each cycle. **e**, Plot of horizontal (x) positions of floats as the machine moves up, showing good agreement between experiment and calculations. **f**, Schematic of the resulting three-stranded braid, showing the braid word at top. Moving the machine cyclically enables the braid word to be repeated because the floats do not swap on the down stroke. **g**, Scanning electron micrograph (SEM) of a three-strand braid, made using the machine in **a** and consisting of Kevlar filaments about 10 µm in diameter.

machine that requires no asymmetric junctions (Extended Data Fig. 1a,b and Supplementary Video 7). The three-strand machine is compact (Extended Data Fig. 1c) because no asymmetric junctions or additional channels are needed (Extended Data Fig. 1d).

To address the second difficulty—that the braid topology is encoded in the shape of the machine—we take advantage of the freedom to reverse the motion of the machine at any height. We create a reversal-activated switch by combining three asymmetric junctions (Fig. 4d). Reversing the motion of the machine when a float is in the operational zone of the switch sends it through a special channel (Supplementary Video 8), which can be used to steer the float through an alternative path.

Switches enable the sequence of swaps to be coded in software (defining the motion of the stage) instead of in hardware (the 3D-printed machine). To demonstrate, we create a single machine that can make any four-strand braid word (Extended Data Fig. 2 and Supplementary Discussion). The machine contains switches that are connected to rotators. When a float is in the operational zone of a switch, reversing the motion of the machine causes the float to enter the rotator. Entering from one direction results in a swap σ_i, and entering from the other results in σ_i^{-1} (Extended Data Fig. 2a). Because the operational zones of each set of switches do not overlap along the vertical axis (Extended Data Fig. 2b), only the neighbouring floats enter a rotator when the switch is activated. The other floats do not swap.

In effect, we 'dial' swaps as in a rotary phone, moving from the starting position to the operational zone of a switch and then back, repeating this process for each desired swap (Supplementary Video 9). Even non-repeating braid words can be made this way, making the machine potentially useful for recording information in a non-volatile way[23].

We assemble these machines from pre-printed modules (Extended Data Fig. 2c,d). We find that the seams between the sections do not affect the functionality of the machine. The modularity enables an even faster way to design and build capillary machines than 3D-printing alone.

Design space and potential applications

An immediate application of these machines is braiding nano- to micro-scale wires for super-high and extremely high-frequency (3–300 GHz) conductors and antennas. In general, high-frequency conductors can be made from filaments with diameters comparable to the electrical skin depth. These filaments are then braided into 'Litz' wire to minimize losses due to proximity effects[24,25]. Litz conductors operating at GHz frequencies require filaments smaller than 10 µm in diameter[13,26,27]. We have shown that capillary machines can braid such small filaments (Supplementary Discussion). The switching machine could be used to make the required braid topologies. Similar capillary machines might be used to make mechanical composites[28–30] or woven textiles that incorporate functional nanofibres.

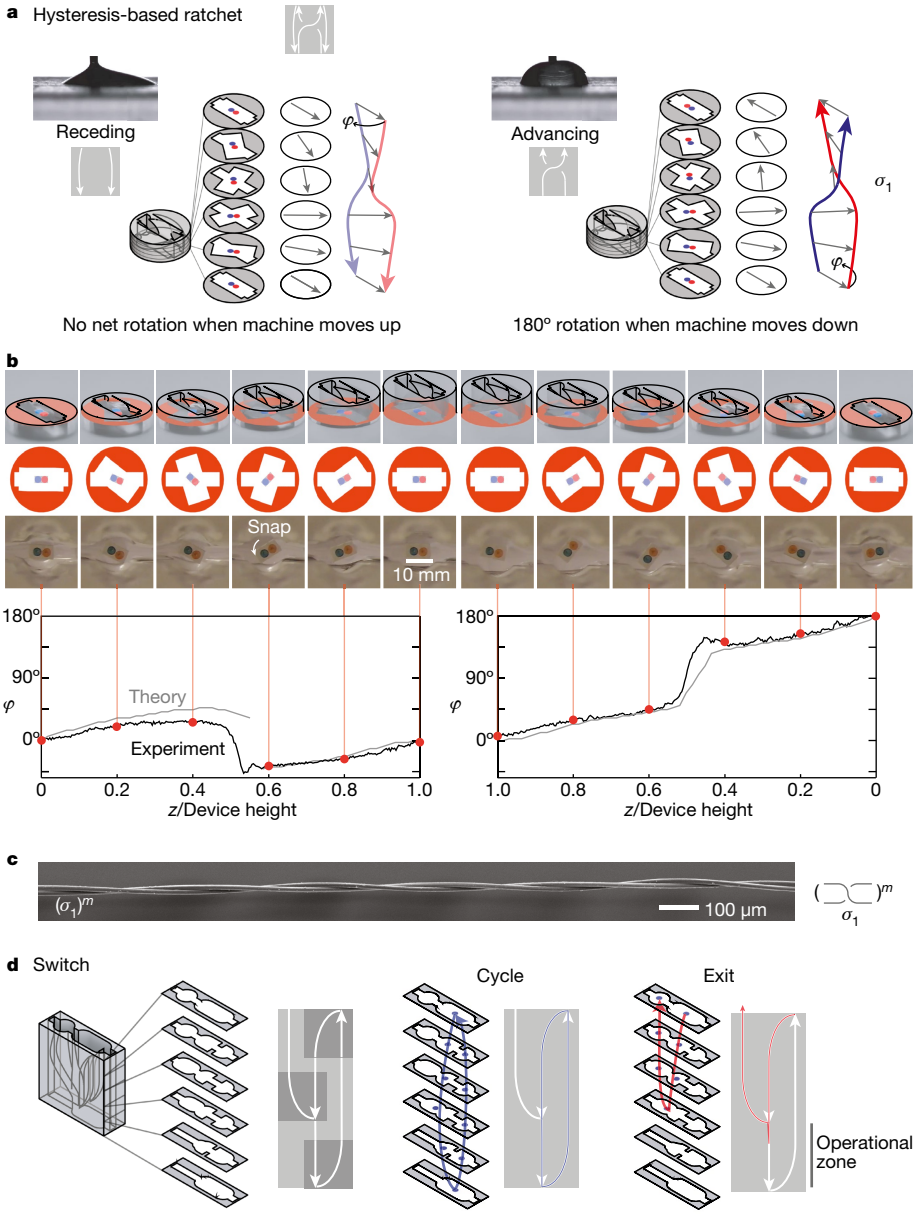

Fig. 4 | Hysteresis and switches enable the design of compact machines. **a**, A machine consisting of a slot and a rectangular channel swept and rotated along the axis acts as a ratcheting rotator, owing to contact-angle hysteresis. As the machine moves up, the contact angle at the walls is the receding angle (photograph). A rectangular float (orientation indicated by the orange and blue circles) tends to align with the slot. As a result, no net rotation of the float occurs, as shown by the cross-sections and illustrated float paths. As the machine moves down, the contact angle corresponds to the advancing angle. The float tends to align with the rectangular channel. As a result, it rotates 180°. **b**, Renderings and top-view images demonstrate the effect of hysteresis on the orientation of the float. Plots of float angle (measured in the right-handed coordinate system illustrated in **a**) as a function of normalized machine level show good agreement between experiment and calculations. **c**, SEM of a two-strand twist, made by attaching two Kevlar filaments about 10 µm in diameter to the float of the machine shown in **a**. **d**, A reversal-activated switch consists of three asymmetric junctions, as shown in the cross-sections and schematics. Different paths are selected by reversing the motion within the 'operational zone' of the switch. As the machine completes a cycle, a float (blue circle) that starts in the first asymmetric junction traces out a cyclical path. Reversing the motion of the machine in the operational zone causes the float to exit this cycle and enter a different channel.

Other applications could be developed to take advantage of the controlled lateral forces exerted by a capillary machine. To investigate the potential applications, we calculate the restoring force in a capillary tweezer as a function of the design parameters. The design parameters (Extended Data Fig. 3a) include: (1) the size of the floats; (2) the contact angle at the wall, controlled by changing or functionalizing the machine material; and (3) the normal force on the float, controlled by changing the float size or density or by adding a weight. We also develop an approximate theory that predicts the trap stiffness, which relates the restoring force to the lateral displacement in the linear regime, and the range of stable operation.

The theory, valid for large capillary lengths, is in qualitative agreement with numerical results obtained for intermediate capillary lengths (Extended Data Fig. 3b–d). Because the contact line at the float can

satisfy different boundary conditions[31], the range of stability may be larger than predicted. When we assume that the contact line is pinned to the top edge of the float, theory and numerical calculations predict that the float is unstable when no weight is added, contrary to our observations (Supplementary Discussion). Roughness at the edge of the float may be responsible for the stability of the real system[32]. The microstructure of the float boundary may therefore represent another design variable.

This caveat aside, we calculate that the trap stiffness can be tuned over six orders of magnitude by changing the contact angle at the wall and the size of the float (Extended Data Fig. 3e). For 10-μm floats, the predicted stiffness is comparable to that of an optical tweezer (approximately 10^{-3} μN mm^{-1}) operating on a similarly sized spherical particle[33].

We find that capillary machines can indeed manipulate such small particles. Our experiments show that rafts of 50-μm silica spheres can be trapped and rotated (Extended Data Fig. 4, Supplementary Discussion and Supplementary Video 10), and individual 20-μm polystyrene spheres can be trapped and translated using a centimetre-scale machine (Extended Data Fig. 5 and Supplementary Discussion, Supplementary Video 10).

Conclusions and future work

Capillary machines are distinct from other classes of machines in that the objects to be manipulated are coupled through a meniscus. The plastic channels do not directly contact the floats; they serve only to modulate the forces exerted by the meniscus. Therefore, even when the objects to be manipulated are microscopic, the shapes of the channels need only be controlled on scales comparable to the capillary length (a few millimetres), which is why functional machines can be made using 3D printing. Compared to machines with other types of linkages, such as mechanical[34], optical[7,8], dielectrophoretic[35], magnetic[36] and fluidic[37,38] micromanipulators, capillary machines are easier to make and can operate on many objects simultaneously. Furthermore, development time is short: a new functional machine can be designed, printed, and tested within a day, making it possible to rapidly develop solutions to other applications. Future work might consider incorporating other forces, including electromagnetic and flow fields[39], to manipulate objects in 3D.

Online content

Any methods, additional references, Nature Research reporting summaries, source data, extended data, supplementary information, acknowledgements, peer review information; details of author contributions and competing interests; and statements of data and code availability are available at https://doi.org/10.1038/s41586-022-05234-7.

1. Bowden, N., Terfort, A., Carbeck, J. & Whitesides, G. M. Self-assembly of mesoscale objects into ordered two-dimensional arrays. *Science* **276**, 233–235 (1997).
2. Tien, J., Breen, T. L. & Whitesides, G. M. Crystallization of millimeter-scale objects with use of capillary forces. *J. Am. Chem. Soc.* **120**, 12670–12671 (1998).
3. Liu, I. B., Sharifi-Mood, N. & Stebe, K. J. Capillary assembly of colloids: interactions on planar and curved interfaces. *Annu. Rev. Condens. Matter Phys.* **9**, 283–305 (2018).
4. Yao, L. et al. Near field capillary repulsion. *Soft Matter* **9**, 779–786 (2012).
5. de Gennes, P.-G., Brochard-Wyart, F. & Quéré, D. *Capillarity and Wetting Phenomena: Drops, Bubbles, Pearls, Waves* (Springer, 2004); https://doi.org/10.1007/978-0-387-21656-0.
6. Vella, D. & Mahadevan, L. The "Cheerios effect". *Am. J. Phys.* **73**, 817–825 (2005).
7. Ashkin, A., Dziedzic, J. M., Bjorkholm, J. E. & Chu, S. Observation of a single-beam gradient force optical trap for dielectric particles. *Opt. Lett.* **11**, 288–290 (1986).
8. Moffitt, J. R., Chemla, Y. R., Smith, S. B. & Bustamante, C. Recent advances in optical tweezers. *Annu. Rev. Biochem.* **77**, 205–228 (2008).
9. Ho, I., Pucci, G. & Harris, D. M. Direct measurement of capillary attraction between floating disks. *Phys. Rev. Lett.* **123**, 254502 (2019).
10. Artin, E. Theory of braids. *Ann. Math.* **48**, 101–126 (1947).
11. Branscomb, D., Beale, D. & Broughton, R. New directions in braiding. *J. Eng. Fibers Fabrics* **8**, 11–24 (2013).
12. Kyosev, Y. *Braiding Technology for Textiles* (Woodhead, 2014).
13. Phillips, J. P. Carbon nano tube Litz wire for low loss inductors and resonators. US patent 8,017,864 (2011).
14. Marchand, P. et al. Braiding mechanism and methods of use. US patent 8,261,648 (2012).
15. Giszter, S., Kim, T. G. & Ramakrishnan, A. Method and apparatus for braiding micro strands. US patent 8,534,176 (2013).
16. Head, A. A. & Ivers, V. M. Rapidly configurable braiding machine. US patent application 14/959,661 (2016).
17. Duwel, A., LeBlanc, J., Carter, D. J. & Kim, E. S. Directed assembly of braided, woven or twisted wire. US patent application 15/248,238 (2017).
18. Quick, R., Thress, C. & Ulrich, G. Braiding machine and methods of use. US patent application 16/754,830 (2020).
19. Zhang, M., Atkinson, K. R. & Baughman, R. H. Multifunctional carbon nanotube yarns by downsizing an ancient technology. *Science* **306**, 1358–1361 (2004).
20. Murnen, H. K., Rosales, A. M., Jaworski, J. N., Segalman, R. A. & Zuckermann, R. N. Hierarchical self-assembly of a biomimetic diblock copolypeptoid into homochiral superhelices. *J. Am. Chem. Soc.* **132**, 16112–16119 (2010).
21. Lu, Y. et al. Braiding ultrathin Au nanowires into ropes. *J. Am. Chem. Soc.* **142**, 10629–10633 (2020).
22. Joanny, J. F. & de Gennes, P. G. A model for contact angle hysteresis. *J. Chem. Phys.* **81**, 552–562 (1984).
23. Sun, G., Liu, J., Zheng, L., Huang, W. & Zhang, H. Preparation of weavable, all-carbon fibers for non-volatile memory devices. *Angew. Chem.* **125**, 13593–13597 (2013).
24. Howe, G. W. O. & Mather, T. The high-frequency resistance of multiply-stranded insulated wire. *Proc. R. Soc. Lond. A* **93**, 468–492 (1917).
25. Hurley, W. G., Duffy, M. C., Acero, J., Ouyang, Z. & Zhang, J. Magnetic circuit design for power electronics. In *Power Electronics Handbook* (ed. Rashid, M. H.) 571–589 (Elsevier, 2018); https://doi.org/10.1016/B978-0-12-811407-0.00019-2.
26. Schulz, M. J. et al. New applications and techniques for nanotube superfiber development. In *Nanotube Superfiber Materials* (eds Schulz, M. J. et al.) 33–59 (William Andrew, 2014).
27. Aydin, A. *Electrospun Polymer Nanofiber Scaffolds for Functionalized Long Sub-micron Diameter Cables*. PhD thesis, Harvard Univ. (2019).
28. Lima, M. D. et al. Electrically, chemically, and photonically powered torsional and tensile actuation of hybrid carbon nanotube yarn muscles. *Science* **338**, 928–932 (2012).
29. Foerster, S. A. & Clemente, S. Optimized suture braid. US patent application 10/803,455 (2006).
30. Ayranci, C. & Carey, J. 2D braided composites: a review for stiffness critical applications. *Compos. Struct.* **85**, 43–58 (2008).
31. Singh, P. & Joseph, D. D. Fluid dynamics of floating particles. *J. Fluid Mech.* **530**, 31–80 (2005).
32. Mao, Z.-S., Yang, C. & Chen, J. Mathematical modeling of a hydrophilic cylinder floating on water. *J. Colloid Interface Sci.* **377**, 463–468 (2012).
33. Malagnino, N., Pesce, G., Sasso, A. & Arimondo, E. Measurements of trapping efficiency and stiffness in optical tweezers. *Opt. Commun.* **214**, 15–24 (2002).
34. Zhang, Z., Wang, X., Liu, J., Dai, C. & Sun, Y. Robotic micromanipulation: fundamentals and applications. *Annu. Rev. Control Robot. Auton. Syst.* **2**, 181–203 (2019).
35. Wang, X.-B., Huang, Y., Gascoyne, P. R. C. & Becker, F. F. Dielectrophoretic manipulation of particles. *IEEE Trans. Ind. Appl.* **33**, 660–669 (1997).
36. Tanase, M., Biais, N. & Sheetz, M. Magnetic tweezers in cell biology. In *Methods in Cell Biology* Vol. 83 (eds Wang, Y.-L. & Discher, D. E.) 473–493 (Academic, 2007).
37. Schneider, T. M., Mandre, S. & Brenner, M. P. Algorithm for a microfluidic assembly line. *Phys. Rev. Lett.* **106**, 094503 (2011).
38. Shenoy, A., Rao, C. V. & Schroeder, C. M. Stokes trap for multiplexed particle manipulation and assembly using fluidics. *Proc. Nat. Am. Soc.* **113**, 3976–3981 (2016).
39. Liu, Y. et al. Manipulation of nanoparticles and biomolecules by electric field and surface tension. *Comput. Meth. Appl. Mech. Eng.* **197**, 2156–2172 (2008).

Methods

We present here a summary of the experimental, theoretical and numerical methods. A full description of the methods and materials used in the experiments, along with all numerical and analytical results and derivations, is presented in the Supplementary Information.

Experimental methods and materials

We designed machines using computer-aided design software (AutoCAD) and printed them using stereolithography-based 3D printers (Form 2 and Form 3, Formlabs). Before operation, machines were cleaned in a plasma cleaner for 1–2 min. To move machines vertically, we placed them on a motorized stage in an acrylic tank filled with distilled water.

Floats were cut from polydimethylsiloxane (SYLGARD 184 PDMS, Dow Chemical Company). 20-μm Fluoresbrite YG polystyrene microspheres were purchased from Polysciences Inc., and 50-μm Fluorescein-isothiocyanate-labelled silica beads were purchased from Nanocs Inc. Fibres with a diameter of 5 to 10 μm were separated by hand from black Kevlar 'magician's thread' purchased from the Thread Exchange.

To use these machines to manipulate fibres, we punctured the silicone floats with acupuncture-style steel needles (0.25 mm diameter and 75 mm length, Peace Classic) and glued one end of each fibre to a needle. We glued the other ends to a weight serving as an anchor. To manipulate microspheres, we used a spreading solvent containing 60% v/v isopropyl alcohol in water to deposit particles at the fluid interface.

To characterize the repulsive capillary forces, we built an apparatus consisting of a vertical fibre optic (radius 110 μm, Thorlabs), a 3D-printed channel, and a tank of water. The fibre and channel were mounted vertically so that they extended through the water–air interface, and a float was attached to the fibre such that the float was at the interface and in the centre of the channel. The fibre was coupled to an LED, and the deflection of the spot emitted by the fibre was measured as the channel was translated horizontally. In this way, the fibre served as a calibrated end-loaded cantilever for measuring the repulsive capillary force between the channel and float.

We used the sessile-drop method on a goniometer (DSA100, KRÜSS GmbH) to measure the contact angle formed at the walls of the machines, and we used a laser line scanner (PT-G 60-40-58, MTI ProTrak) to measure the profile of the meniscus. The results of these characterization techniques are discussed in full detail in the Supplementary Information.

We used a Samsung NX 10 camera and a Samsung 18–55 mm OIS lens to take videos and photos of the floats during operation of the machines. Braids and twists of microscale fibres were imaged with a Zeiss FESEM Ultra Plus scanning electron microscope. We used an Apple iPhone 8 to take videos of microspheres moving during operation of the machines. The microspheres were illuminated with blue light (440 nm peak wavelength) from a SPECTRA X light engine (Lumencor) and imaged through a bandpass filter (Brightline Multiband Filter 387-485-559-649, Semrock) that blocks the excitation wavelength. Rafts of microspheres were imaged with a Dino-Lite Edge (5MP Series) digital microscope.

Theoretical and numerical modelling

To model the motion of the floats in a capillary machine, we reduced the full three-dimensional problem to a series of two-dimensional boundary value problems (BVPs). In this approach, each cross-section of the machine along its axis of motion is treated independently as a function of height. The cross-section at a given height then provides the geometry of the outer boundary $\partial\Omega_o$ of the BVP, with outwards normal n. The inner boundary $\partial\Omega_i$ is provided by the float, which is initially placed at an arbitrary position and configuration within the channel. Between these two boundaries, the meniscus surface h satisfies the following Helmholtz equation, obtained by minimizing the gravitational potential, surface tension, and adhesion energy of the fluid to the channel wall[5]:

$$\nabla^2 h - \ell^{-2} h = 0,$$
$$\text{with } \nabla_n h = c \text{ on } \partial\Omega_o \text{ and } h(s) = z(s) \text{ on } \partial\Omega_i.$$

Here ℓ is the capillary length. The outer boundary condition (BC) is a Neumann BC which can be interpreted as a constant contact slope c at the channel wall. The inner BC is a Dirichlet BC resulting from the pinning of the meniscus to the float edge $z(s)$. In deriving this equation, we assumed that the float was fixed in space. To predict the trajectory of the float during machine operation, we relaxed this assumption and allowed the system to minimize the total energy across all positions and orientations of the float. Doing so as a function of height yielded the trajectory that a float or multiple floats take through the machine.

For numerical results, the solution of the BVP was carried out via the finite-element method as implemented in MATLAB's PDE Toolbox. The optimization was done via Nelder–Mead optimization as implemented in MATLAB's fminsearch function. We used MATLAB v2018b for these calculations.

Data availability

Raw videos and experimental data are available on the Harvard Dataverse (https://doi.org/10.7910/DVN/9AHDUL).

Code availability

The code for tracking floats from videos, processing surface profilometry data, and processing restoring force measurement data can be found at https://github.com/Faaborg/float_tracker and Zenodo (https://doi.org/10.5281/ZENODO.6916546). The code for numerical calculations of float motion can be found at https://github.com/falkma/capillarymachines-numerics and Zenodo (https://doi.org/10.5281/ZENODO.6816029). CAD files for 3D printing the machines in this paper are available at https://github.com/manoharan-lab/capillary-stl and Zenodo (https://doi.org/10.5281/ZENODO.6909015).

Acknowledgements We thank A. Duwel, D. J. Carter, K. J. Russell, R. Gordon, A. Aydin, C. Chang, R. Garmann and Z. Rozynek for helpful discussions and D. Clarke and J. Aizenberg for use of equipment. This work was supported by Defense Advanced Research Projects Agency (DARPA) contract FA8650-15-C-7543 to the Charles Stark Draper Laboratory. It was supported in part by NSF through the Harvard University Materials Research Science and Engineering Center, grant DMR-2011754. Additional support was provided by NSF through grant ECCS-1541959, the Office of Naval Research through grant number N00014-17-1-3029, and the Simons Foundation.

Author contributions Y.B.-S. conceived the capillary tweezer. C.Z. and M.W.F. conceived capillary machines that use the tweezer to control the paths of multiple floats. C.Z. designed and built the motorized stage, controller and tank. C.Z., M.W.F. and A.S. designed, built and tested all the capillary machines and did all the experiments on the machines. C.Z., M.W.F., A.S., M.J.F. and R.H. developed the hysteresis-based mechanism for swapping. M.W.F. and V.N.M. conceived the switch and arbitrary braiding machine, and C.Z., M.W.F. and A.S. designed and built these machines. C.Z. did the SEM imaging. M.X. measured the contact angles, surface tension and meniscus profile. K.H. measured the capillary forces. M.J.F., R.H., Y.B.-S. and M.P.B. developed the theory and numerical approach and did all the simulations. M.J.F. developed the perturbative theory and did the design-space calculations. M.W.F. analysed the float trajectories. M.W.F., A.S. and V.N.M. wrote the main text and made the figures, based on initial drafts by C.Z., M.W.F. and V.N.M. and incorporating input from all authors. All authors wrote the Supplementary Information. A.S. created the videos. V.N.M. oversaw all experimental work and preparation of the paper. M.P.B. oversaw all theoretical and numerical work. V.N.M. and M.P.B. obtained funding for the work.

Competing interests A US patent application (application serial number 17/639,088) on the design of capillary machines that manipulate and assemble micro- and nanoscopic objects has been filed by C.Z., M.W.F., A.S., Y.B.-S., M.P.B. and V.N.M.

Additional information
Supplementary information The online version contains supplementary material available at https://doi.org/10.1038/s41586-022-05234-7.
Correspondence and requests for materials should be addressed to Vinothan N. Manoharan.
Peer review information *Nature* thanks Camille Duprat, Shigeki Saito and the other, anonymous, reviewer(s) for their contribution to the peer review of this work. Peer reviewer reports are available.
Reprints and permissions information is available at http://www.nature.com/reprints.

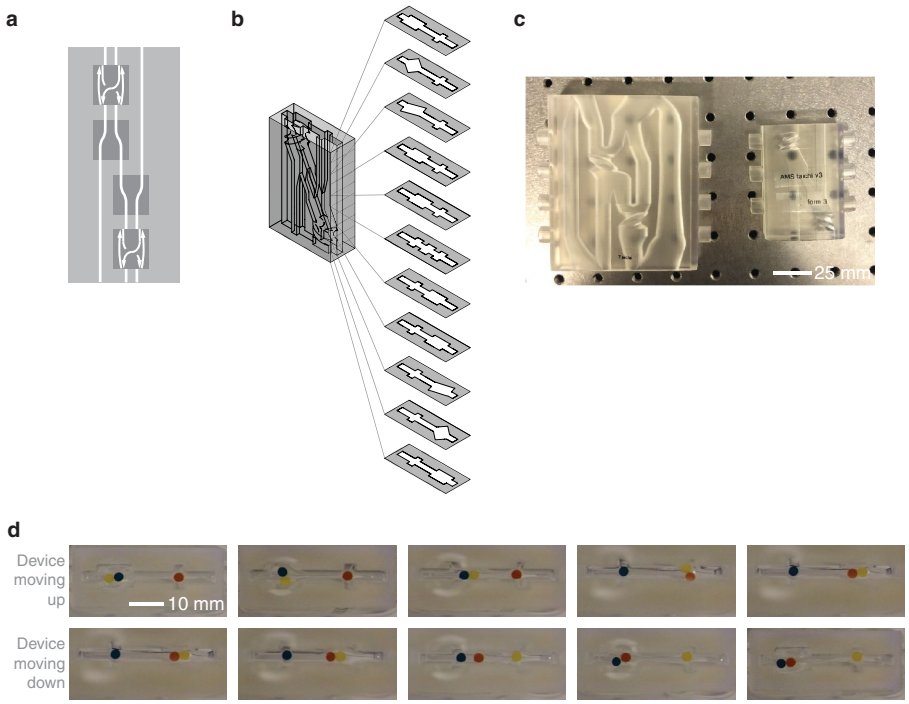

Extended Data Fig. 1 | A braiding machine using contact-angle hysteresis. **a**, A schematic of a machine that uses hysteresis-based ratchets to braid fibres, without any asymmetric junctions. **b**, A diagram of the machine with cross-sections shown on the right. **c**, Photograph of the three-strand braiding machine shown in Fig. 3 (left) and the hysteresis-based braiding machine (right). Both machines make the same braid, with the same number of fibres, but the hysteresis-based machine is much more compact. **d**, Top-view photographs of the machine and floats. As the machine moves up, the three floats execute two swaps to make a $\sigma_1\sigma_2^{-1}$ braid. As the machine moves back down, the floats do not swap positions. The resulting braid is the same as that shown in Fig. 3.

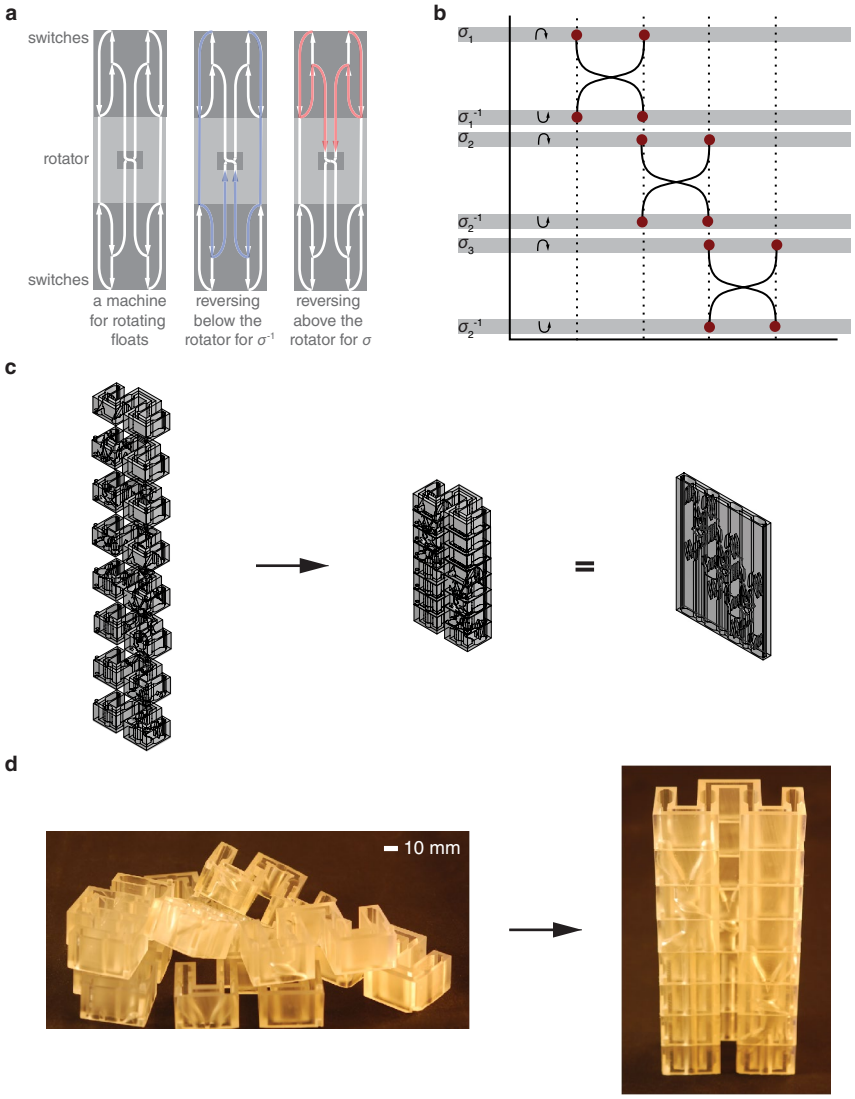

Extended Data Fig. 2 | Machines to make arbitrary braid words. a, A schematic showing how a single rotator, connected to four reversal-activated switches, enables a pair of floats to be swapped in two ways. Two switches are above the rotator and two below, as shown in the left diagram. If the motion of the machine is reversed in the operational zone of the bottom switches, the floats complete a σ^{-1} swap, as shown by the blue arrows in the centre diagram. If the motion of the machine is reversed in the operational zone of the top switches and then reversed again, the floats complete a σ swap, as shown by the red arrows in the right diagram. **b**, Diagram of a four-strand braiding machine consisting of three vertically staggered copies of the machine shown in **a**. Black paths represent rotators, and grey bars represent heights at which the machine can be reversed to swap different pairs of floats. The reversal of the machine can therefore be used to select any σ_i or any σ_i^{-1}. **c**, Diagram of a four-strand arbitrary braiding machine that has been modified ('folded') to reduce its horizontal extent and that has been divided into eight horizontal slices that can slide into each other. The modified design is equivalent to a 'flat' four-strand arbitrary braiding machine (right). **d**, Photographs of a four-strand braiding machine as separate parts (left) and combined to form a single machine (right).

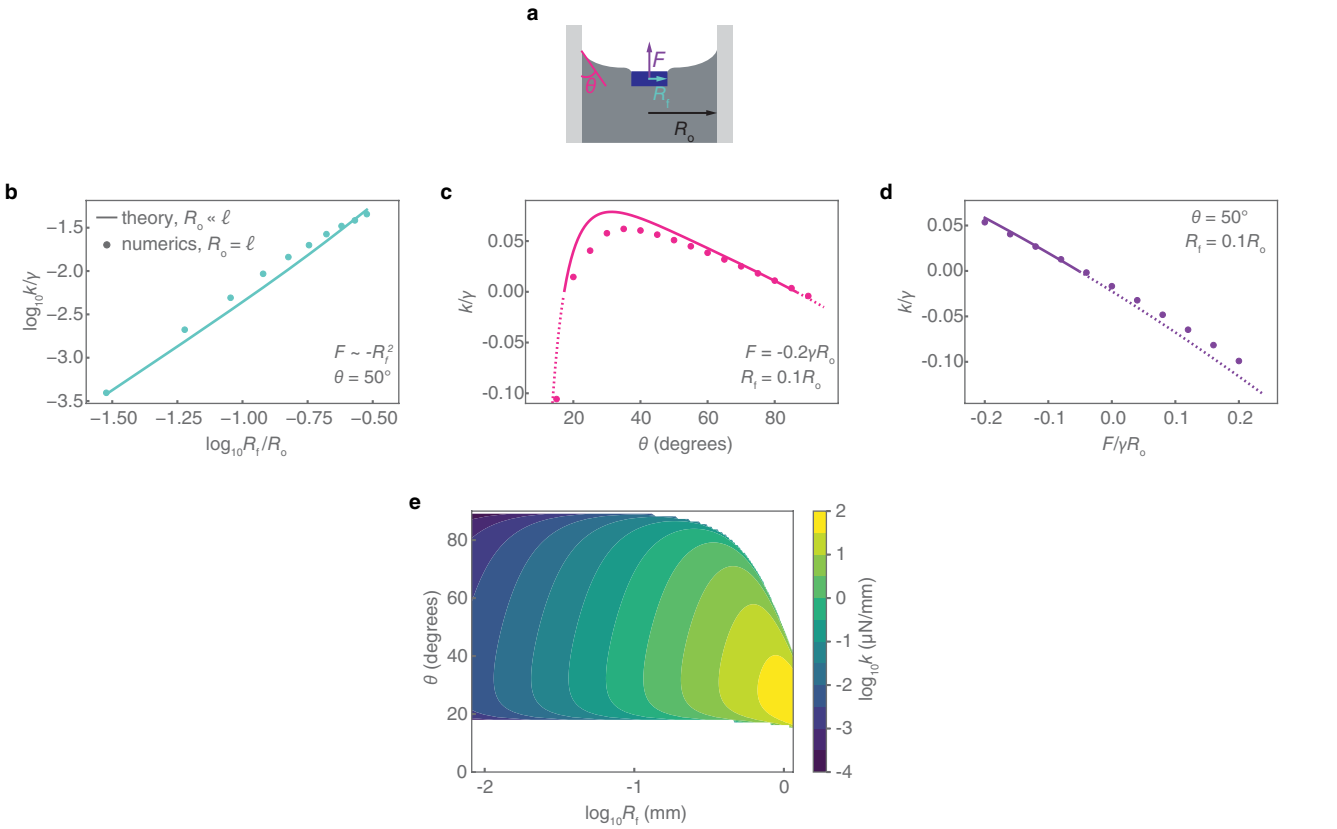

Extended Data Fig. 3 | The design space of a capillary tweezer. a, Diagram of a capillary tweezer showing the contact angle at the wall (θ), float radius (R_f), normal force (F), and channel radius (R_o). **b**, Plot of nondimensionalized tweezer stiffness (k/γ) as a function of R_f/R_o for a contact angle of 50°, and a negative F that scales with R_f^2. Circles show numerical calculation and solid line shows calculation from perturbative theory. The perturbative theory assumes that $\ell \gg R_o$, while all numerical calculations are performed with $R_o = \ell$. **c**, Plot of nondimensionalized trap stiffness as a function of contact angle for a float with $R_f = 0.1R_o$ and a normal force $F = -0.2\gamma R_o$. At very small or very large contact angles the trap stiffness becomes negative (dotted line), meaning that the float does not stably follow the centre of the channel. **d**, Plot of nondimensionalized trap stiffness as a function of nondimensionalized normal force for a contact angle of 50° and a float with $R_f = 0.1R_o$. **e**, Heatmap of trap stiffness as a function of float radius and contact angle from perturbative theory. White areas correspond to where the tweezer is unstable. See Supplementary Information for further details.

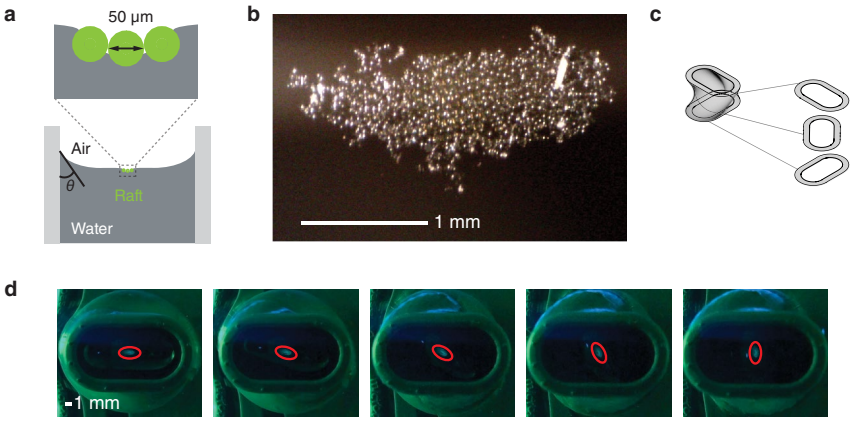

Extended Data Fig. 4 | Rotating rafts of microscopic particles with a capillary machine. a, Diagram of 50-µm-diameter silica particles assembling into a raft under the influence of the mutual capillary attraction between them. The raft bends the interface downwards, allowing it to be trapped in the centre of a hydrophilic channel. **b**, An optical micrograph of a typical raft made in an oval channel taken from above. **c**, Diagram of a centimetre-scale rotator used to rotate the raft. **d**, Photographs of the machine taken from above show the raft (circled in red) rotating as the height of the machine changes. See also Supplementary Video 10.

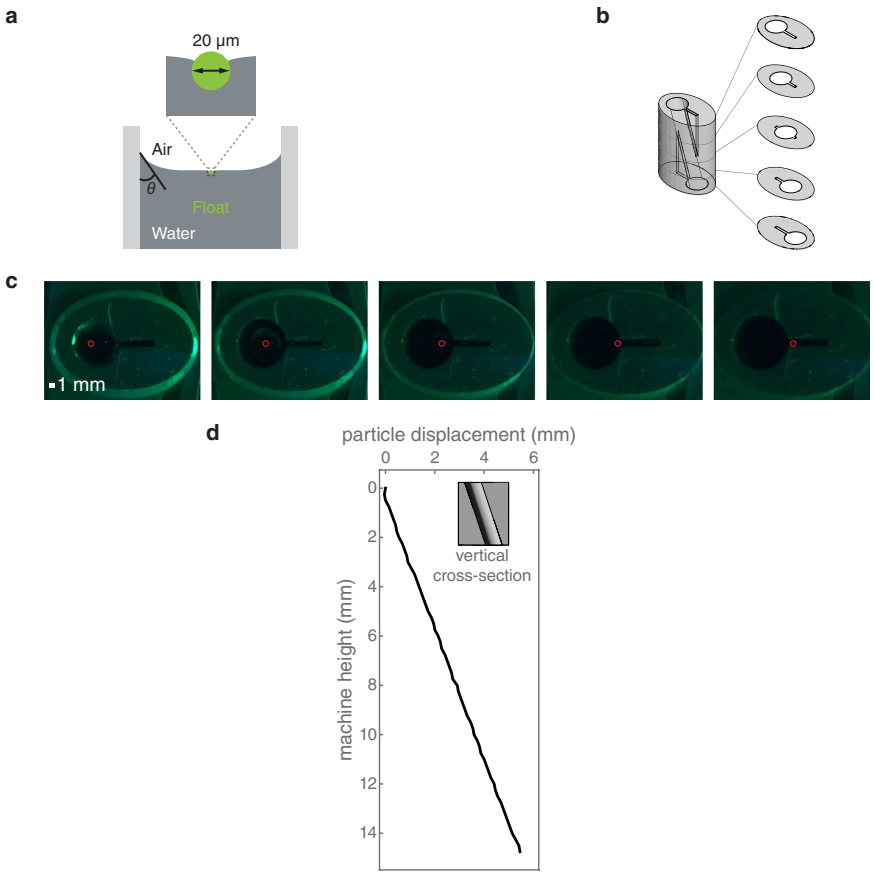

Extended Data Fig. 5 | Manipulating microscopic particles with a capillary machine. a, Diagram of meniscus formed when water fills a hydrophilic channel with contact angle θ. A polystyrene sphere with a diameter of 20 µm and that is denser than water bends the interface downwards (inset). **b**, A diagram of a centimetre-scale machine with a sloping channel used to translate a microscopic particle. **c**, Photographs of the machine taken from above show the 20-µm-diameter particle (circled in red) moving as the height of the machine changes. See also Supplementary Video 10. **d**, Measured particle displacement as a function of machine height, alongside a diagram of the vertical cross-section of the machine taken along its centre (inset).